Cure-dependent Viscoelastic Poisson's Ratio of Epoxy

D.J. O'Brien · N.R. Sottos · S.R. White

Abstract The evolution of the lateral contraction ratio of two commercial (high and low temperature cure) epoxy resins is studied in uniaxial tension using moiré interferometry. The ratio of transverse to axial strains evolves from an elastic value of about 0.40 to a rubbery plateau value of 0.49 at long times. Furthermore, the data indicate that the contraction ratio follows time-temperature superposition with a shift function indistinguishable from other axial viscoelastic functions. The lateral contraction behavior at several cure states past gelation was measured and a model is proposed to describe the cure dependence.

Keywords Viscoelasticity · Poisson's ratio · Cure-dependence · Moiré interferometry

D.J. O'Brien (✉)
Department of Mechanical and Industrial Engineering,
University of Illinois at Urbana-Champaign, Urbana,
IL 61801, USA
e-mail: dobrien@arl.army.mil

Present Address:
D.J. O'Brien
Weapons and Materials Research Directorate,
US Army Research Laboratory, Aberdeen Proving Ground,
Aberdeen, MD 21005, USA

N.R. Sottos (SEM member)
Department of Materials Science and Engineering,
University of Illinois at Urbana-Champaign, Urbana,
IL 61801, USA

S.R. White (SEM member)
Department of Aerospace Engineering,
University of Illinois at Urbana-Champaign, Urbana,
IL 61801, USA

Introduction

The Poisson's ratio of an isotropic viscoelastic solid is time dependent [1] as are the other material functions such as the tensile and bulk relaxation moduli. This matrix time-dependent behavior of the Poisson's ratio has a significant effect on certain micromechanical predictions of composite viscoelastic relaxation. Yet, experimental characterization of the viscoelastic Poisson's ratio is quite difficult, requiring the measurement of at least two independent viscoelastic functions. Furthermore, simultaneous measurement of these functions gives more accurate results since derivative properties can be calculated without introducing errors due to specimen and environmental variation.

Although a wealth of data have been collected on the viscoelastic response of polymers in shear and extension, data on the time dependence of the Poisson's relaxation of polymers are lacking. Several studies present time-dependent Poisson's ratio data. However, the data are limited to low temperature [2–6], large strains [7–9], or the experimental technique is applicable to only certain materials [10]. An early work by [11] presents only instantaneous values for the Poisson's ratio of polymers at large strains.

Tsou et al. [12] attempted to infer the viscoelastic Poisson's ratio of various polymer films from independent experiments in bending and tension. For polycarbonate, the calculation resulted in non-monotonic behavior with an initial value near 0.40, a peak of 0.45 and a long time value of about 0.34. While the authors point out that this type of behavior is technically feasible, it is not expected and was likely due to the method's sensitivity to error as Poisson's ratio approaches 0.5 [1].

Recently [13] used epoxy-bonded strain gages to measure the dynamic Poisson's ratio of a urethane adhesive. Unfortunately, the gages significantly reinforced the specimen and required that the data be corrected for reinforcement effects. The shift factor of the dynamic Poisson's ratio could not be obtained from their data since the epoxy adhesive and polyimide gage backing may have altered the time-dependent behavior, especially at high temperature.

Ernst et al. [14] also used strain gaged specimens in their study, an investigation of an electronic packaging molding compound's time-dependent Poisson's ratio. The tensile and lateral creep compliances of specimens were measured and converted to viscoelastic Poisson's ratio. Because the equilibrium modulus of the molding compound is above 1 GPa, it is likely that the gages did not significantly reinforce the specimens. However, time-temperature superposition of the Poisson's ratio data failed and it was unclear if the failure was a result of the inaccuracy of the data or non-thermorheologically simple material behavior.

Lu et al. [15] utilized image moiré to measure the time dependence of the Poisson's ratio of poly(methyl methacrylate). Unfortunately the image moiré technique is not able to adequately resolve the transverse strains, and as a result their data were quite noisy. Kugler et al. [16] used a novel optical technique, with transverse resolution better than 1 μm, to simultaneously measure axial and transverse strains in filled rubber. Stress relaxation measurements were performed to measure the time dependent relaxation modulus and Poisson's ratio at various strain levels (1–20%). Shift factors employed to construct master curves for both material functions were identical.

In other studies, Theocaris [17, 18] measured the time dependence of the Poisson's ratio in creep and stress relaxation of EPON 828 epoxy cured with triethylenetriamine using geometric moiré with gratings of 20 lines per millimeter. Although the experimental curves presented for Poisson's ratio are 'smooth,' details on the data analysis are lacking. From the configuration specified, the authors claim that the strain measurement is accurate to 10 $\mu\epsilon$ over a gauge length of ∼ 10 mm. These results are suspect since such resolution would require resolving fringe orders to the third decimal place.

The scarcity of adequate measurements of the viscoelastic response of Poisson's ratio is likely due to the difficulty associated with characterizing the two-dimensional deformation of rubbery materials with common experimental techniques. In this paper, we report on a series of moiré interferometry experiments to measure the creep compliance and time dependent

Poisson's ratio simultaneously over a range of temperatures. Two epoxy polymers are investigated: a fully reacted bisphenol A-based system with relatively low T_g and a high T_g bisphenol F system at several cure states past gelation.

Theory of the Viscoelastic Poisson's Ratio

Viscoelastic Analog of the Poisson's Ratio

The Poisson's ratio, ν, of an isotropic elastic material is defined as,

$$\epsilon_2 = -\nu\epsilon_1 \tag{1}$$

where ϵ_1 and ϵ_2 are the material's axial and transverse strains in uniaxial deformation. For an elastic material in tension the transverse strain will obviously be the same in either a stress-controlled (creep-type) or strain-controlled (stress relaxation-type) experiment. It follows from the correspondence principle that the Poisson's ratio of a linear viscoelastic isotropic material is defined in the Laplace domain as [1],

$$\epsilon_2(s) = -s\bar{\nu}(s)\bar{\epsilon}_1(s) \tag{2}$$

where the bar over a function denotes the Laplace transform. If a stress relaxation experiment is considered then equation (2) becomes,

$$\bar{\epsilon}_2(s) = -\bar{\nu}(s)\epsilon_0 \tag{3}$$

where ϵ_0 is the constant strain applied at time, $t = 0$. Taking the inverse Laplace transform of equation (3) and rearranging gives,

$$\nu(t) = \frac{-\epsilon_2(t)}{\epsilon_0} \quad . \tag{4}$$

Equation (4) shows that the viscoelastic Poisson's ratio $\nu(t)$ can be determined directly from a tensile stress relaxation experiment by measuring the transverse strain over time. Additionally, the stiffness $\mathbf{C}$ and compliance $\mathbf{S}$ tensors for a linear viscoelastic material must be related by,

$$\int_{-\infty}^{t} \mathbf{S}(t - \tau)d\mathbf{C}(\tau) = h\mathbf{I} \tag{5}$$

where h is the Heaviside step function and $\mathbf{I}$ is the unit tensor. van der Varst and Kortsmit [19] showed that equation (5) is true only if the viscoelastic Poisson's ratio is given by equation (4). Similarly, [20] also showed

that the correspondence principle is only valid for cases where the viscoelastic Poisson's ratio has the form given in equation (4).

For a creep-type experiment in tension equation (2) still applies. However, since the axial and transverse strains are now time dependent, equation (2) does not reduce to a form that has a simple inverse Laplace transform. Therefore, the ratio of transverse and axial strains,

$$\nu^c(t) = \frac{-\epsilon_2(t)}{\epsilon_1(t)} \qquad (6)$$

is called the *lateral contraction ratio in creep* $\nu^c(t)$ to distinguish it from the viscoelastic Poisson's ratio.

Determination of $\nu(t)$ from $\nu^c(t)$

Since experiments are much easier to perform in creep (constant load) versus stress relaxation (constant displacement), in this study creep experiments were carried out to determine $\nu^c(t)$ which was then converted to $\nu(t)$. In order to make this conversion, note from equation (2) that the axial and transverse strains in a creep experiment can be related to $\nu(t)$ through [1],

$$\epsilon_1(0)\nu(t) - \int_0^\infty \nu(t)\frac{d\epsilon_1(t-u)}{du}du = -\epsilon_2(t) \ . \qquad (7)$$

To solve equation (7), [21] derived the recurrence formula,

$$\nu(t_n) = \frac{-2\epsilon_2(t_n) + \nu(t_{n-1})(\epsilon_1(0) - \epsilon_1(t_n - t_{n-1})) + X(i_n)}{\epsilon_1(0) + \epsilon_1(t_n - t_{n-1})}$$

where

$$X(t_n) = \sum_{i=1}^{i=n-1}(\nu(t_i) + \nu(t_{i-1}))(\epsilon_1(t_n - t_i) - \epsilon_1(t_n - t_{i-1}))$$

$$(8)$$

with,

$$\nu(t_1) = -\frac{2\epsilon_2(t_1) + \nu_g(\epsilon_1(t_1) - \epsilon_1(0))}{\epsilon_1(t_1) + \epsilon_1(0)} \ . \qquad (9)$$

In terms of the creep compliance $D(t)$ and $\nu^c(t)$, equations (8) and (9) become,

$$\nu(t_n) = \frac{2D(t_n)\nu^c(t_n) + \nu(t_{n-1})(D_g - D(t_n - t_{n-1})) + Y(t_n)}{D_g + D(t_n - t_{n-1})}$$

where

$$Y(t_n) = \sum_{i=1}^{i=n-1}(\nu(t_i) + \nu(t_{i-1}))(D(t_n - t_i) - D(t_n - t_{i-1}))$$

$$(10)$$

with,

$$\nu(t_1) = \frac{2D(t_1)\nu^c(t_1) - \nu_g(D(t_1) - D_g)}{D(t_1) + D_g} \qquad (11)$$

where D_g and ν_g denote the glassy compliance and Poisson's ratio, respectively.

Characteristic Times of $\nu(t)$

As a final note on the background of the viscoelastic Poisson's ratio, the proper definition of this function's characteristic time is important for interpretation of the experiments. The characteristic times in an axial creep experiment are called retardation times, λ, because the axial strain never reaches equilibrium. On the other hand, the stress never reaches equilibrium in a stress relaxation experiment, and the characteristic times are called relaxation times. However, while the axial behavior is a relaxation process, the transverse strain in a tensile stress relaxation experiment is a retardation process since it never reaches a constant value. Therefore, the characteristic times of the viscoelastic Poisson's ratio are neither the relaxation nor the retardation times, rather they are called *delay* times, τ^θ [21].

Experimental Procedure

We first begin with a discussion of the principles of moiré interferometry and how strains are measured with this experimental technique. The design of the experimental apparatus is then presented along with details of specimen preparation, testing, and image analysis.

Strain Measurement by Moiré Interferometry

In moiré interferometry, two coherent beams of light are directed towards a reflective grating mounted on the specimen surface. The angle α, measured from the specimen normal, is chosen so that when the specimen is undeformed the $+1$ and the -1 diffraction orders of beams 1 and 2, respectively, fall along a line normal to the specimen. This condition results in a uniformly

bright or dark image at the image plane. When the specimen experiences a strain ϵ the grating frequency becomes,

$$f_s = \frac{f/2}{1 + \epsilon} \qquad (12)$$

and interferometric fringes develop due to a phase shift between the two beams.

The displacement U is related to the fringe order N by,

$$U = \frac{1}{2f} N \qquad (13)$$

and the strain is,

$$\epsilon_1 = \frac{\Delta N}{2f \Delta x} \qquad (14)$$

where Δx is the gage length and ΔN is the change in the number of fringes across the gage length with respect to the reference configuration.

More generally, the strain can be written as,

$$\epsilon_i = \frac{\Delta N_i}{2 f_i \Delta x_i} \quad i = 1, 2 \qquad (15)$$

where the $1-$ and $2-$ ($U-$ and $V-$) directions represent the axial and transverse directions, respectively, in a uniaxial tension experiment.

Experimental Apparatus

A schematic of the experimental setup is shown in Fig. 1. The specimen, with its diffraction grating positioned within the viewing field of the interferometer (Portable Engineering Moiré Interferometer (PEMI), Photomechanics Inc., Vestal, NY), was pin loaded in creep using a dead weight creep apparatus as described by [22]. The creep apparatus was constructed from the pivoted crossbeam of a triple beam balance (700 series, OHaus Co., Pine Brook, NJ). A small piezoelectric load cell (Model 9712A500, Kistler, Amherst, NY) was placed in line with the specimen. The creep apparatus was mounted on a rotation stage which was in turn mounted on a two-axis translation stage for coarse adjustments. Moiré images were recorded with a CCD camera (Model XC-003, Sony Co.). A rail table with a support arm attached was positioned to support the loading weights prior to initiating the creep experiment. The support arm could be lowered remotely to minimize vibrations at the beginning of the experiment. The entire setup was mounted on a pneumatic isolation table to minimize vibrations. A Macintosh computer running LABview (version 5.0, National Instruments, Austin, TX) controlled the CCD camera, recorded the load cell data, and controlled the loading through the position of the support arm attached to the rail table.

For temperature control, the specimen was mounted inside a bath of silicone oil (200 Fluid: 1,000 cSt, Dow-Corning). The bath was constructed of aluminum with a plate glass front to allow for optical access. Two silicone rubber heaters (Watlow, St. Louis, MO) were clamped around the sides of the bath, and temperature control was provided by a PID (series 965, Watlow) controller with a platinum RTD mounted close to the specimen. After stabilizing at the prescribed temperature, the bath could be maintained at that temperature to within $\pm 0.1°$C. Additionally, to mitigate air currents caused by free convection from the oil bath's window, foam baffles were placed between the interferometer and the front side of the oil bath. The baffles were positioned so that they did not block the beams of the interferometer. The entire setup was also covered by a shroud to block currents from the laboratory environment.

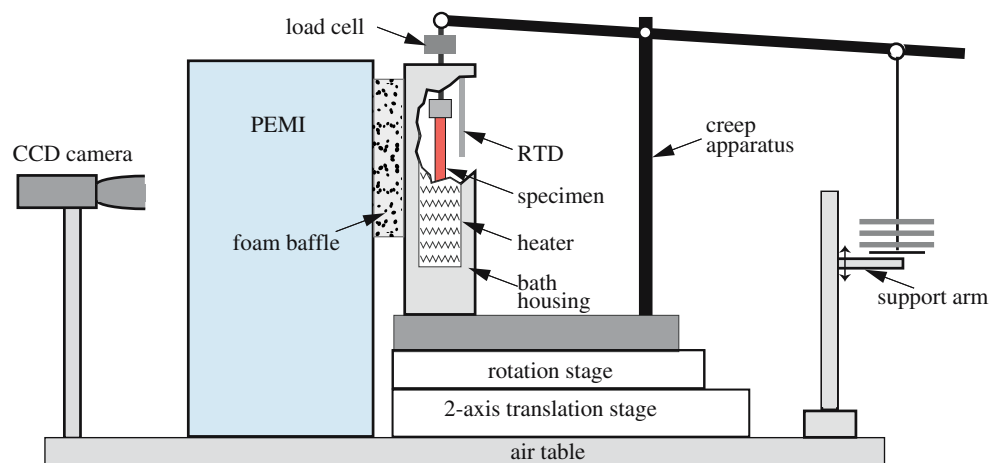**Fig. 1** Schematic of PEMI, creep apparatus, and supporting equipment (shroud not shown)

Table 1 Cure cycles used for manufacturing EPON 862/W creep specimens

Specimen type	Hold temperature(°C)								Degree of cure
	75	100	110	125	150	177	50	177	α
1	600	60	–	60	60	120	1	480	1.0
2	600	60	60	–	–	–	1	–	0.90
3	600	30	–	–	–	–	1	–	0.79

Numbers given are time in minutes spent at each temperature
Temperatures were reached at a rate of 0.5°C/min

Specimen Manufacture

Tensile specimens were manufactured from two different epoxy resin systems. EPON Resin 862 (Shell Chemical, Houston, TX), a bisphenol F epoxide, was cured with EPON Curing Agent W (Shell Chemical, Houston, TX), diethyltoluene diamine. This epoxy cures at high temperature and has a fully cured T_g of $\sim 150°C$. EPON 862/W specimens were manufactured at three different cure states to complement previous work on the cure kinetics [23] and cure-dependent viscoelastic properties [24] of this material. A second system was also investigated, EPON 828/3274, a bisphenol A epoxy and aliphatic amine curing agent that cures at room temperature and has a T_g of $\sim 50°C$.

The diffraction gratings were molded directly into the tensile creep specimens by modifying the procedure outlined in [25]. First a silicone rubber (RTV 615, GE Silicones) submaster mold of a 1,200 line/mm grating (Photomechanics Inc.) was replicated onto a glass substrate. After mixing and thorough degassing, the epoxy resin was poured into open-faced silicone

rubber molds (RTV 630, GE Silicones) nominally 83 $\times$ 12 $\times$ 2 mm. Next, the silicone rubber submaster was carefully placed face down onto the uncured resin. The specimens were then cured according to an appropriate cure cycle. The cure cycles used for the EPON 862/W specimens are shown in Table 1. The EPON 828/3274 specimens were cured for 48 h at room temperature followed by 10 h at 75°C to ensure the material was fully reacted. After curing, aluminum tabs were bonded to the end of the specimens, and a thin layer (~ 10 nm) of indium was evaporated onto the specimen diffraction grating using a thermal evaporator (model CVE 301, Cooke Vacuum Products, Norwalk, CT) equipped with an oscillating quartz thickness monitor (model STM-100/MF, Sycon Industries, East Syracuse, NY). Since the Young's modulus of indium is quite low (10.8 GPa) compared to aluminum (69 GPa) [26], it was chosen as the coating material to avoid artificially stiffening the specimen. Although weak fringe patterns could be detected through the silicone bath without the use of a coating, the attenuation was large enough to require a coating.

Fig. 2 Initial $U-$ field images of EPON 862/W specimens (**a**) cured with MRC and (**b**) cured using Type 1 cycle (Table 1)

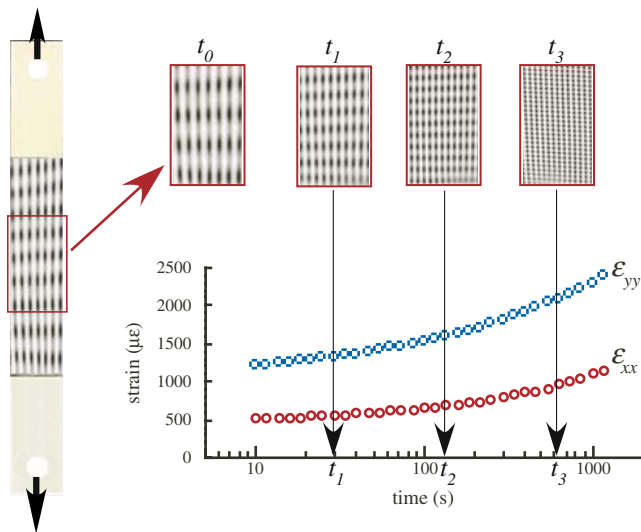
(a)   (b)

Fig. 3 Schematic of moiré images taken at equally spaced intervals in log(*time*)

The fairly unconventional cure cycles used for the EPON 862/W specimens were determined after considerable trial and error. Curing the specimens according to the manufacturer's recommended cure cycle (MRC, 1 h at 121°C and 2.5 h at 177°C) resulted in unsatisfactory gratings that produced initial fringe patterns populated by many irregular fringes. Figure 2 shows typical initial fields of specimens cured with the MRC and the cycle given in Table 1 for full cure (Type 1).

Atomic force microscopy (AFM) was used to verify the frequency of the molded gratings. Analysis of AFM images yielded a grating frequency of $f = 1,202 \pm 9$ lines mm, with negligible bias in the grating frequency $\left(\frac{f_1}{f_2} = 1.001 \pm 0.006\right)$.

Creep Testing

After installing the specimen in the test frame, the tank was filled with silicone oil and the interferometer was tuned so that a minimum of fringes were present in both the $U-$ and $V-$ fields. Carrier fields of extension were then added so that the fringe density was 1 to 2 fringes/mm. The temperature was then allowed to stabilize for approximately 2.5 h. After an image of the initial fields was taken, the specimen was loaded and images were recorded at measurement intervals equally spaced in log(*time*) from 10 to 1,200 s as shown in Fig. 3. At each interval two images were taken 1/30 s apart. The creep load was chosen for a maximum total strain of between approximately 2,000 and 2,500 $\mu\epsilon$. This level of strain was chosen to be small enough so that linearity could be assumed, yet large enough to accurately resolve the relaxation of the contraction ratio.

In moiré experiments, the $U-$ and $V-$ field images are often captured separately because the moiré patterns cannot be easily distinguished from one another. However, in uniaxial tension the displacement field is quite simple manifesting in vertical and horizontal fringes for the $U-$ and $V-$fields, respectively, (Fig. 3). Therefore, a single image is sufficient to resolve both displacement fields.

After the creep test was completed, the load was removed and the silicone oil bath was heated to the next temperature. The temperature was again allowed to stabilize for approximately 2.5 h, and the test was repeated. Since the stabilization time is much greater than the creep interval (20 min), memory of the previous loading history is negligible [27]. Experiments were conducted at temperatures up to $\sim T_g - 15°C$,

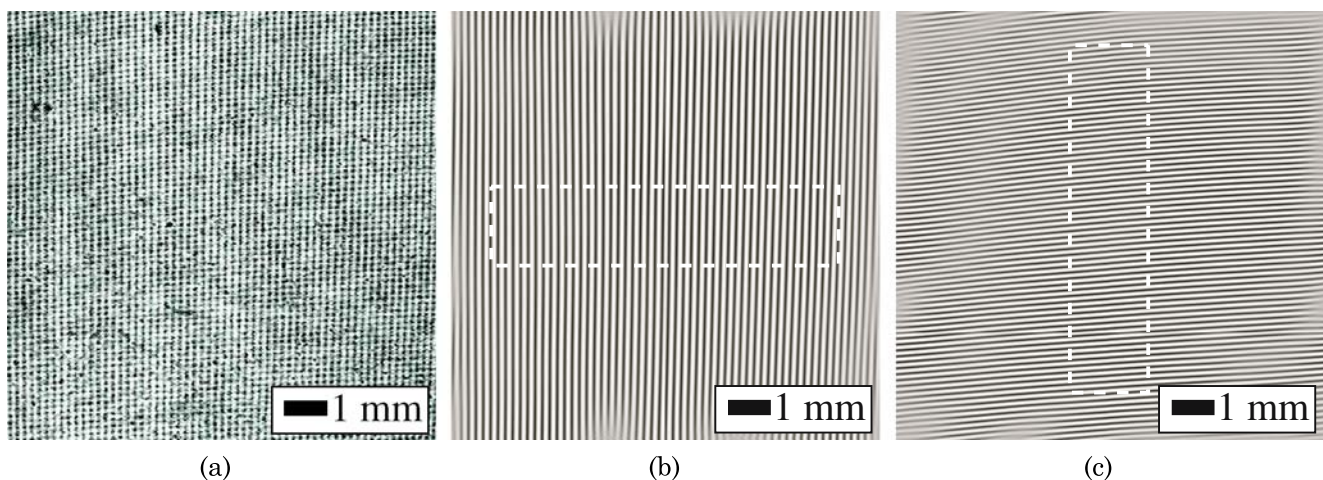**Fig. 4** Image processing of interferograms: (**a**) interferogram of $U-$ and $V-$ fields taken simultaneously; (**b**) $U-$ field after filtering; (**c**)$V-$ field after filtering. Dashed boxes represent typical areas used for calculating fringe density

$\sim T_g$, and $T_g + 20°C$ for the $\alpha = 0.79, 0.90,$ and 1.0 specimens, respectively. The specific test temperatures used are given in the Results and Discussion section with each specimen's respective master curve.

For the experiments on the partially cured samples, a small container holding DSC specimens was placed in the oil bath adjacent to the tensile specimen. After each creep test, a DSC specimen was removed from the container for DSC analysis. Measurements of the specimens' residual heats of reaction revealed no advancement in cure state for either partially cured sample (Type 2 or 3). However, an increase in T_g from 103 to 112°C for the Type 2 specimen ($\alpha = 0.90$) specimen was detected after the experiment at the highest temperature. Cure advancement was prevented in Type 3 since the maximum temperature tested was 15°C below T_g.

Image Processing

After creep testing, the acquired images were processed to determine the axial strain, transverse strain, and lateral contraction ratio. Figure 4(a) shows a typical moiré interferogram. The horizontal fringes represent contours of constant displacement in the axial direction while the vertical fringes represent displacement contours in the transverse direction. Since the displacement field is quite simple, it is possible to separate the $U-$ and $V-$ fields in the Fourier domain. This separation was accomplished using the software package NIH Image (National Institutes of Health, Bethesda, MD). Figures 4b and c show the $U-$ and $V-$fields after filtering.

After separation, the fringe densities were determined by taking scans along a line of pixels in the central portion of the specimen and averaging at least 50 scans about 8 mm in length each. The dashed boxes in Figs. 4(b) and (c) show typical scanned areas. Since two images were taken at each measurement interval, the strains at each interval were determined by averaging the data obtained from each pair of images.

Results and Discussion

Experimental Validation

The experimental apparatus and procedure were designed with care in order to achieve precise temperature control. Since the coefficient of thermal expansion of epoxy is approximately 50 $\mu\epsilon$/°C [28], a simple calculation shows that the measured Poisson's ratio will change by almost 10% if the temperature varies by only

1°C during the experiment. Considering that Poisson's ratio relaxes only about 25% ($0.35 \lesssim \nu(t) \lesssim 0.5$) over the entire range of behavior, precise temperature control is essential during the experiment.

Improved temperature control and faster response could be attained by agitating the bath liquid. Unfortunately, the motion of the fluid caused the specimen to vibrate with respect to the interferometer and created small fluctuations in the temperature between the PEMI and the sample. Thermal fluctuations induce small changes in the index of refraction (of the fluid) which cause the moiré fringes to 'dance' as described by [25].

Fringe dancing can also be caused by air currents between the interferometer and the specimen. These currents can be the result of room circulation or, in the case of the present setup, free convection from a heated vertical surface. During experiments at high temperature (above $\sim 120°C$) the air currents caused by the heated front side of the oil bath caused severe fringe dancing. The use of baffles between the interferometer and the bath as well as a shroud covering the entire setup greatly reduced fringe dancing.

Unfortunately, fringe dancing could not be eliminated completely and progressively noisier data resulted as temperature increased. As a result, it was difficult to verify the validity of time-temperature superposition for the lateral contraction ratio using EPON 862/W, a high temperature epoxy. Since the T_g of EPON 828/3274 is low ($\sim 50°C$), the transition region of the viscoelastic response can be measured at much lower temperatures than EPON 862/W. Thus,
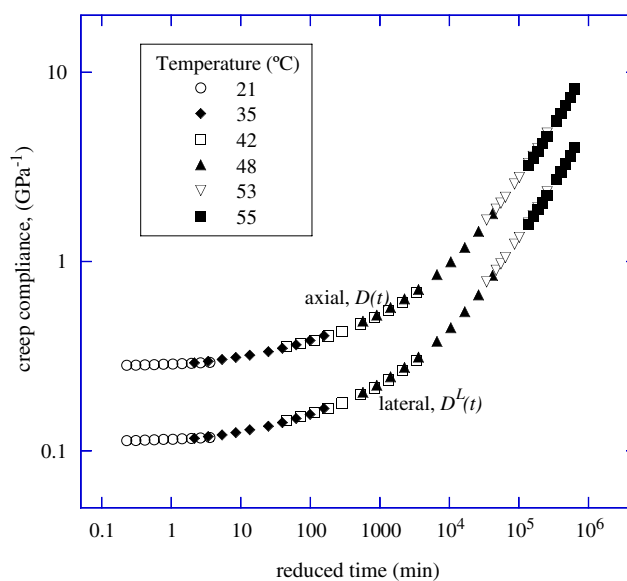

Fig. 5 Creep compliance master curves for EPON 828/3274 epoxy ($T_{ref} = 21°C$)

the lateral contraction ratio data of EPON 828/3274 are much smoother through this transition, and these data were analyzed first to confirm time-temperature superposition and provided guidance in analyzing the EPON 862/W data.

EPON 828/3274

A room temperature curing epoxy, EPON 828/3274, was tested in axial creep experiments. Figure 5 shows master curves for the axial and lateral creep compliances defined as,

$$\text{axial:} \quad D(t) = \frac{\epsilon_1(t)}{\sigma_0} \quad , \tag{16}$$

$$\text{lateral:} \quad D^L(t) = \frac{-\epsilon_2(t)}{\sigma_0} \quad . \tag{17}$$

Here, the lateral creep compliance is chosen as the second viscoelastic material function instead of the contraction ratio since it changes by several orders of magnitude while the contraction ratio only changes by about 25% during creep. Thus, the lateral compliance appears less noisy than the contraction ratio making it more convenient to shift.

Shifting these creep compliances according to time-temperature superposition reveals that excellent superposition can be obtained if identical horizontal a_T and vertical b_T shift factors are used for both material functions (see Fig. 6). While the vertical shift factor is small and not absolutely necessary for good superposition, we include it to explore how vertical shifting of the compliances affects the contraction ratio master curve.
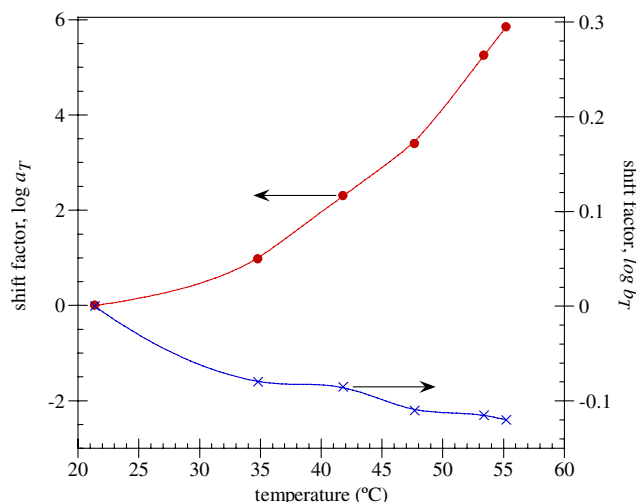
Fig. 6 Horizontal (a_T) and vertical (b_T) shift factors used in constructing compliance master curves for EPON 828/3274 epoxy
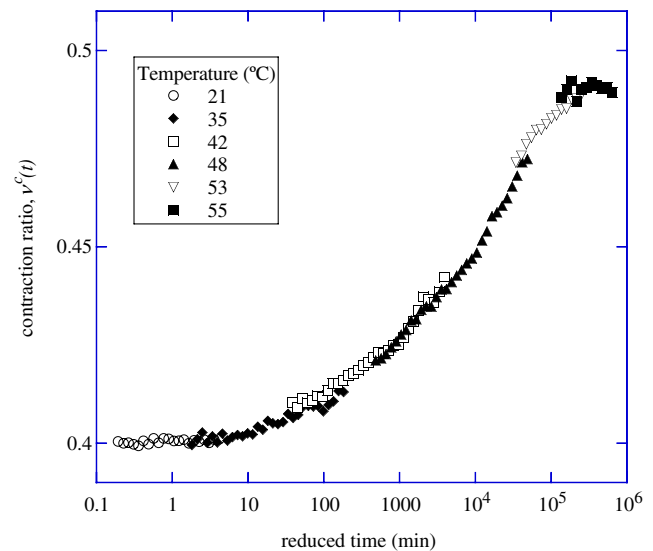
Fig. 7 Lateral contraction ratio in creep master curve for EPON 828/3274 epoxy ($T_{ref} = 21°C$)

The lateral contraction ratio in creep can be defined in terms of the unshifted and shifted compliances as,

$$\nu^c(t, T) = \frac{D^L(t)}{D(t)} = \frac{b_T^L D^L(a_T^L t, T_o)}{b_T D(a_T t, T_o)} \tag{18}$$

where a_T^L and b_T^L are the shift factors associated with the lateral creep compliance and a_T and b_T are the shift factors associated with the axial creep compliance.

In order for time-temperature superposition (TTS) to be valid, all viscoelastic material functions must have the same shift factors. As equation (18) shows, since the axial and transverse creep compliances have identical shift factors TTS is at least phenomenologically appropriate for the lateral contraction ratio. Identical shift factors for the two compliances also means that the contraction ratio will have the same horizontal shift function as the creep compliance and that vertical shifting is not required.

Figure 7 shows lateral contraction ratio data after horizontal shifting. Excellent superposition and a smooth curve is obtained over the entire temperature range studied with $\nu^c(t)$ relaxing from a glassy value of 0.4 to almost 0.5.

EPON 862/W

The high temperature structural epoxy (EPON 862/W) was then analyzed, having established that the lateral contraction ratio obeys time-temperature superposition and that an accurate master curve can be constructed using the same horizontal shift factors as those obtained for axial creep compliance. Results are presented for both fully and partially cured samples.
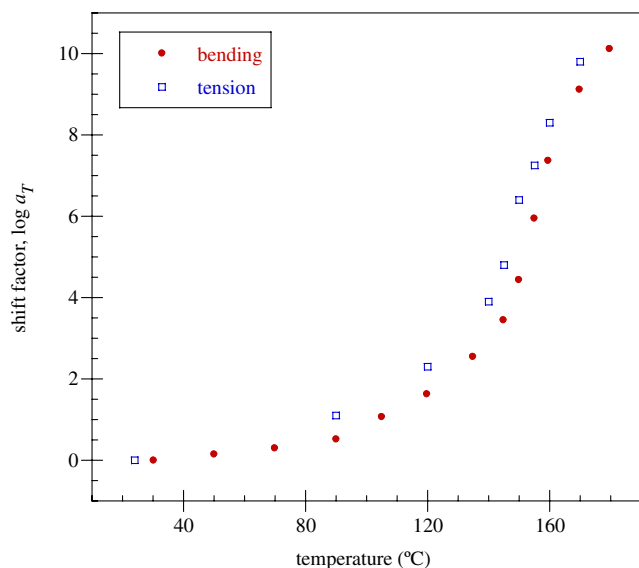
Fig. 8 Shift factors used in constructing creep compliance master curves from three-point bending [24] and tensile data (for EPON 862/W)

Full cure

The axial creep behavior of the material in tension was first examined and compared to earlier work on the same material in three-point bending [24]. Figure 8 shows the shift factors used to construct creep compliance master curves from the tensile and three-point bending data while Fig. 9 compares the resulting master curves for the creep compliance in three-point bending and tension. The shift factors are similar, but the shift factors from the tensile (moiré) experiments are slightly higher than those from three point bending. Also, the
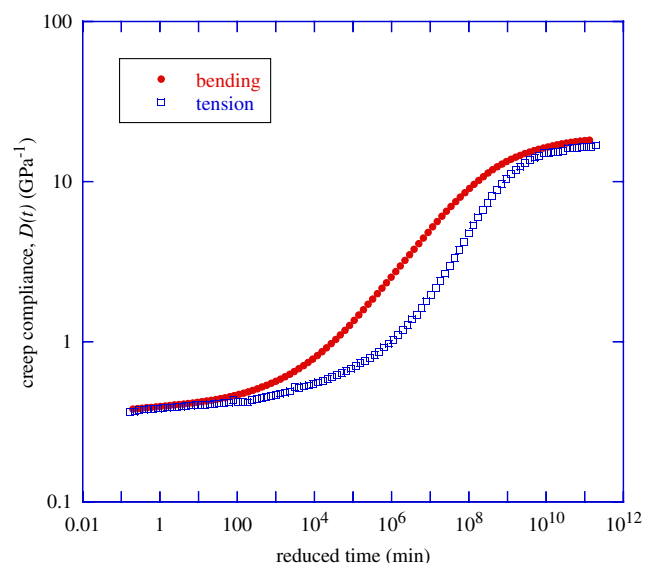

Fig. 9 Creep compliance of EPON 862/W determined from three-point bending [24] and tension ($T_{ref} = 30°C$)
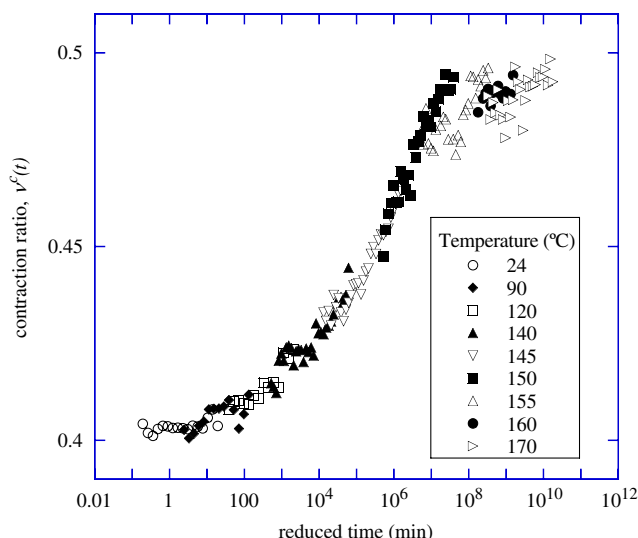

Fig. 10 Lateral contraction ratio in creep for EPON 862/W. Master curve was developed using same shift factors as creep compliance data ($T_{ref} = 24°C$)

behavior of the creep compliance in tension is different than that in three-point bending. While the two functions agree well in the glassy and rubbery regions, the tensile creep compliance relaxes more slowly than that determined from three-point bending.

The difference in relaxation behavior is likely due to differences in the aging protocol. The three-point bending experiments were performed with a new specimen at each temperature and the experiment started as soon as the environmental chamber equilibrated. Conversely, the tensile experiments were performed after a very long equilibration time at the test temperature. Although the similarity between the rubbery moduli suggests similarity of the crosslink densities, the difference in relaxation behavior could also be due to the difference in the cure cycles used to manufacture the two specimen types. Additionally, the difference in stress state between the two experiments could contribute to a difference in relaxation behavior. Drozdov [29] found

Table 2 Coefficients and delay times for viscoelastic Poisson's ratio of EPON 862/W ($T_{ref} = 24°C$)

i	$\log[\tau_i^{\theta}(\min)]$	ν_i^c	ν_i
g		0.4925	0.4925
1	2	−0.00693	−0.00709
2	3	−0.01182	−0.01212
3	4	−0.00896	−0.00905
4	5	−0.01927	−0.02098
5	5.8	−0.02225	−0.02594
6	6.6	−0.01287	−0.00842
7	7.5	−0.00213	−0.00167
8	9.5	−0.00512	−0.00403

Table 3 Coefficients and retardation times for tensile creep compliance of EPON 862/W ($T_{ref} = 24°C$)

i	$\log[\lambda_i(\text{min})]$	D_i (GPa^{-1})
0		0.03641
1	0	0.03154
2	1	0.01711
3	2	0.02942
4	3	0.03063
5	4	0.09320
6	5	0.13184
7	6	0.50287
8	7	0.79918
9	8	4.58360
10	9	9.53330
11	10	0.06995

that the relaxation rate decreases from torsion to compression to tension. It is also possible that a difference in environmental conditions of the two experiments resulted in a variation in the measured behavior. In any case, the difference also emphasizes the point that it is difficult to determine multiple viscoelastic material functions from independent experiments.

Figure 10 shows shifted lateral contraction ratio data for the fully cured EPON 862/W. Unfortunately, due to fringe dancing the data get progressively noisier as temperature increases. Nevertheless, good superposition is also achieved if the same horizontal shift factors are used for the tensile creep compliance and lateral contraction ratio.
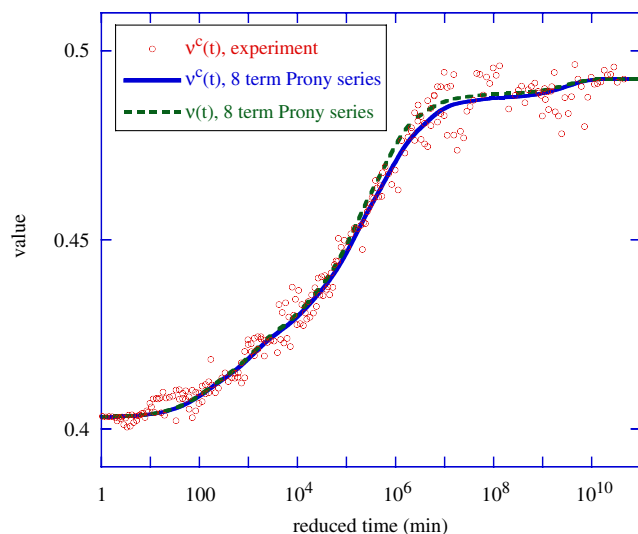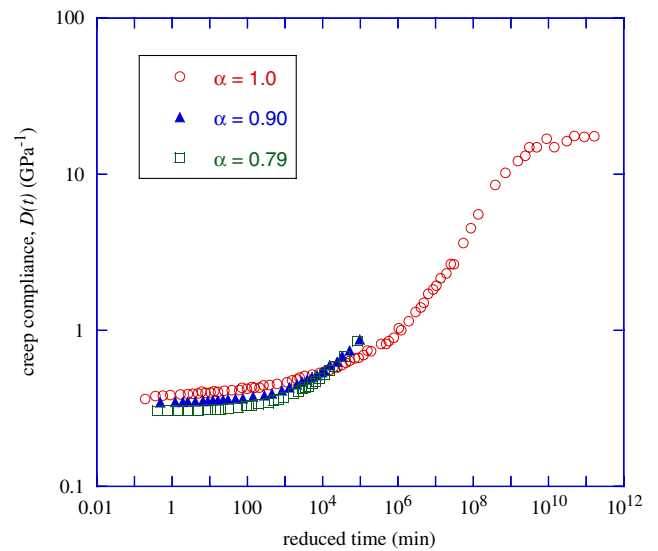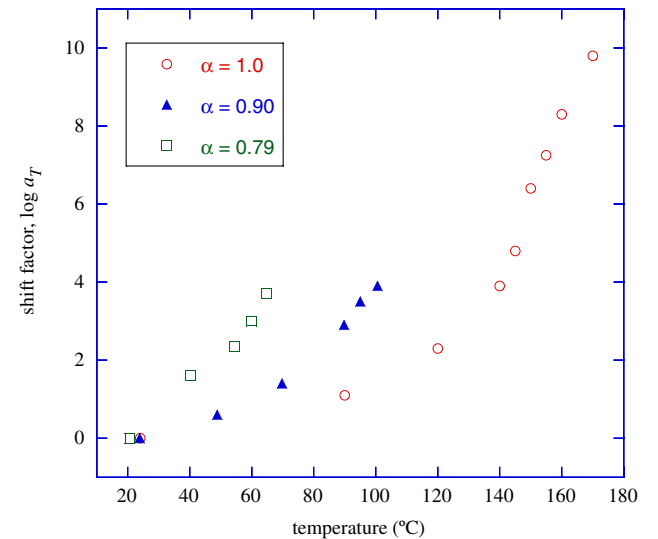

Fig. 11 Lateral contraction ratio master curve for EPON 862/W fit to an eight-term Prony series and converted to viscoelastic Poisson's ratio ($T_{ref} = 24°C$)

(a)

(b)

Fig. 12 Creep compliance (**a**) and shift factors (**b**) of EPON 862/W at various cure states. Master curves were constructed with shift factors identical to those used to construct lateral contraction ratio master curves in Figs. 10, 13(a) and 13(b) ($T_{ref} = 24°C$)

Conversion to viscoelastic Poisson's ratio

To convert the fully cured lateral contraction ratio in creep data to the viscoelastic Poisson's ratio, the $\nu^c(t)$ data were fit to an eight-term Prony series (Table 2),
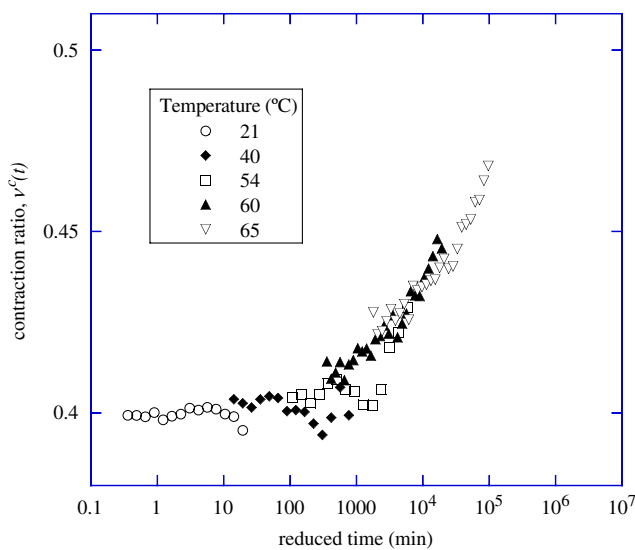
$$\nu^c(t) = \nu_g + \sum_{i=1}^{8} \nu_i^c \exp\left(\frac{-t}{\tau_i^\theta}\right) \qquad (19)$$
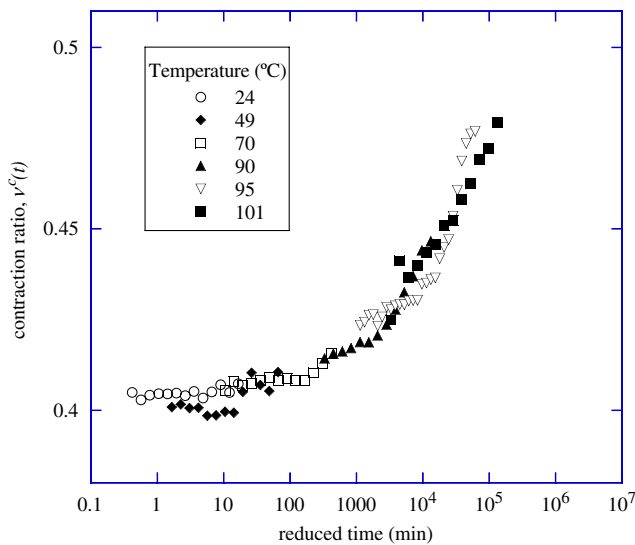
and the tensile creep compliance was fit to an 11-term generalized Voigt model (Table 3),

$$D(t) = D_0 + \sum_{i=1}^{11} D_i \left[1 - \exp\left(\frac{-t}{\lambda_i} \right) \right] . \qquad (20)$$

Equations (19) and (20) are then used with equation (10) to determine the viscoelastic Poisson's ratio from this analysis. Since the data taken at high temperatures are quite noisy, the equilibrium value was taken as the average of the last ten data points, yielding $\nu_g = 0.493 \pm 0.004$. Figure 11 shows the lateral contraction ratio in creep and the viscoelastic Poisson's

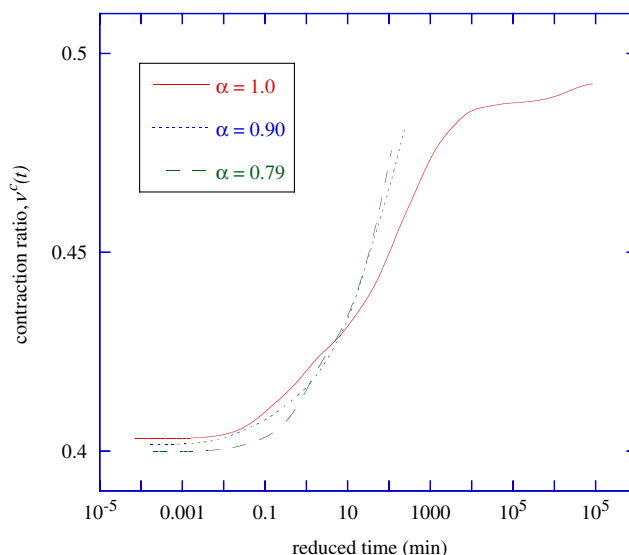**Fig. 14** Lateral contraction ratio for EPON 862/W at various cure states past gelation ($T_{ref} = T_g - 20°C$)

ratio. There is little difference between the two except the Poisson's ratio relaxes slightly faster near the end of the transition. As with the longitudinal and shear functions, faster relaxation under constant displacement compared to constant load is expected since the relaxation function is simply the material response of a single strain increment whereas the creep function is the superposition of many successive strain increments. Since the contraction ratio monotonically increases as it relaxes, it follows that in this superposition the creep response will lag behind the relaxation behavior. The viscoelastic Poisson's ratio shown in Fig. 11 was also fit to an eight-term Prony series (Table 2).

Partial cure

EPON 862/W samples were also tested at partially cured conditions for $\alpha = 0.79$ and $\alpha = 0.90$. Since the networks are only partially formed, the relaxation is accelerated compared to full cure. The creep compliance master curves are shown in Fig. 12(a) along with the shift factors used in their construction, Fig. 12(b). The data for the partially cured samples only extend partially through the transition to preclude effects of cure advancement at elevated temperature.

The lateral contraction ratio of the partially cured samples is shown in Figs. 13(a) and (b). The shift factors used in their construction are the same as the creep compliance data. Again, the contraction ratio begins in the glassy state at about 0.4 and quickly increases during relaxation to values approaching 0.5.

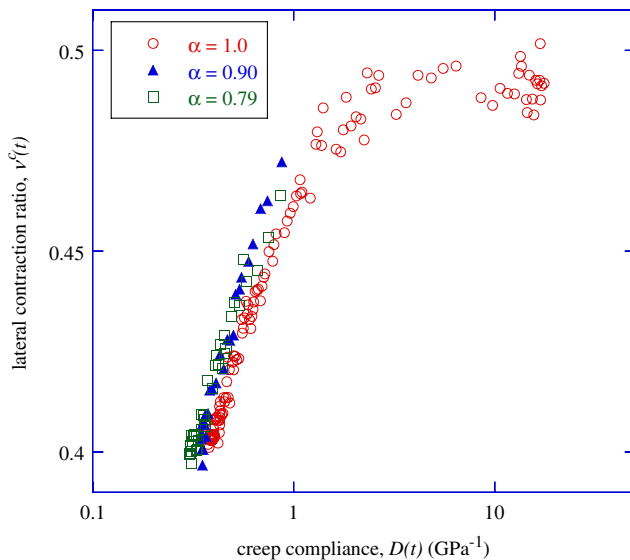To compare the development of the lateral contraction ratio across cure states, the master curves

(a)

(b)

Fig. 13 Time-temperature superposition of lateral contraction ratio data for EPON 862/W, (**a**) $\alpha = 0.79$ ($T_{ref} = 21°C$) and (**b**) $\alpha = 0.90$ ($T_{ref} = 24°C$)

Fig. 15 Lateral contraction ratio in creep for EPON 862/W plotted versus creep compliance at several cure states ($T_{ref} = 24°C$)

are shifted to a common reference temperature with respect to T_g. This allows for comparison of the time-dependent material behavior without including temperature effects. Figure 14 shows the lateral contraction ratio master curves at various cure states with reference temperatures of $T_{ref} = T_g - 20°C$. Because the data are fairly noisy, only the smoothed master curves are shown. Similar to the creep compliance and relaxation modulus, the elastic response of the contraction ratio is essentially insensitive to cure state. Also, the transition region becomes progressively steeper
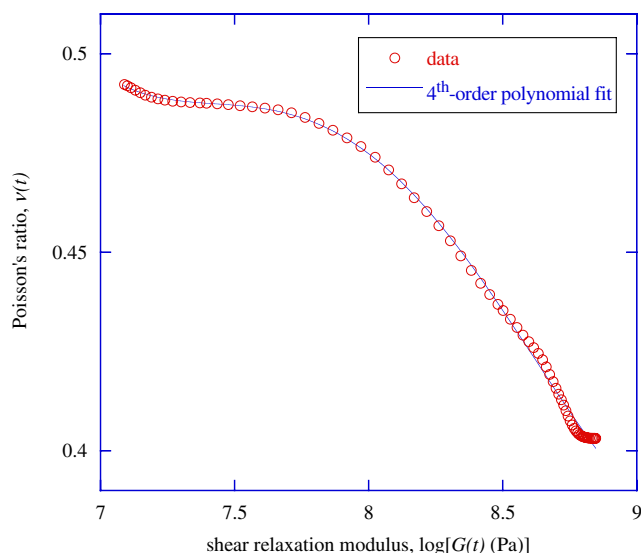

Fig. 16 Relationship between shear relaxation modulus and viscoelastic Poisson's ratio at full cure for EPON 862/W. Circles represent data and line is 4th order polynomial fit ($T_{ref} = 30°C$)

Table 4 Polynomial coefficients for relating $v(t, \alpha)$ and $G(t, \alpha)$

i	$g_i \; ([log(\text{Pa})]^{-i})$
0	116.07
1	−58.463
2	11.044
3	−0.92288
4	0.028759

For $G > 10^7$ Pa, $v(t) = \sum_{i=0}^{4} g_i [\log G(t)]^i$; for $G < 10^7$ Pa, $v(t) = 0.4925$

with decreasing cure state indicating that the breadth of the relaxation decreases with cure state.

Cure-dependent Viscoelastic Poisson's Ratio

It is clear that the state of cure has a profound impact on the viscoelastic behavior of epoxy [24] including Poisson's ratio (Fig. 14). Modeling this effect for Poisson's ratio in the context of equation (19) requires that the change in Prony series coefficients, $v_i(\alpha)$, and delay times, $\tau_i^\theta(\alpha)$, be described over the entire range of cure. Unfortunately, $v^c(t, \alpha)$ data could only be collected in the later stages of cure ($\alpha > 0.79$) for the moiré technique. Instead of resorting to extrapolation over the full range of cure extent, we assume that the viscoelastic Poisson's ratio and the creep compliance develop in the same manner with cure state. In this case the cure dependence of the Poisson's ratio can be found by cross-plotting the Poisson's ratio and creep compliance at a common cure state (α^*) so that $v(t, \alpha^*) = f[D(t, \alpha^*)]$. If the Poisson's ratio and creep compliance depend on cure state in the same manner then the function f is the same for all cure states α^*, and a cross plot should show that the data collapse onto one curve.

The creep compliance and lateral contraction ratio data are plotted against one another in Fig. 15 at the cure states tested. The data collapse onto a single curve within the bounds of experimental scatter and generally supports the assumption of identical cure dependence.

An explicit model for the cure dependence of the Poisson's ratio is obtained by plotting the viscoelastic Poisson's ratio at full cure, Fig. 16, versus the fully cured shear relaxation modulus, $G(t)$, determined in a previous study [24]. This curve was fit empirically using a fourth-order polynomial to obtain the scaling function between Poisson's ratio and shear relaxation modulus, i.e. $v(t, \alpha) = g[G(t, \alpha)]$. The coefficients of this relationship are listed in Table 4.

Since the relaxation modulus data lie above about 10^7 GPa, extrapolating the polynomial outside this region could yield unrealistic results (i.e. $v > 0.5$). As

such, the Poisson's ratio is assumed to have reached equilibrium ($v = 0.4925$) when the shear relaxation modulus falls below about 10^7 Pa. The equilibrium value of the Poisson's ratio is also assumed to be independent of cure, a reasonable assumption since the equilibrium Poisson's ratio is 0.4925 at full cure. While the equilibrium value might be expected to increase with decreasing cure state as the material behaves more like a fluid, the Poisson's ratio cannot exceed 0.5 and the experimental resolution is not sufficient to differentiate such small differences in Poisson's ratio.

Conclusions

A method using moiré interferometry was developed for simultaneously measuring the axial and transverse strains of polymers in tension through T_g. The technique proved to be accurate enough to measure the small strains necessary for determining the lateral contraction ratio while overcoming difficulties associated with strain measurement of soft materials. The technique was used to measure the lateral contraction ratio in creep of room and elevated temperature cured epoxies. The lateral contraction of the two epoxies exhibited significant viscoelastic behavior. The data show that the viscoelastic Poisson's ratio can be shifted according to time-temperature superposition using the same horizontal shift factors as the creep compliance. Finally, a study of the cure dependence of the lateral contraction past gelation revealed that the material behavior can be reasonably modeled as a function of the relaxation modulus irrespective of cure state.

References

1. Tschoegl NW, Knauss WG, Emri I (2002) Poisson's ratio in linear viscoelasticity–a critical review. Mech Time-depend Mater 6:3–51.
2. Bogy DB, Bugdayci N, Talke FE (1979) Experimental determination of creep functions for thin orthotropic polymer films. IBM J Res Develop 23(4):450–458.
3. Yee AF, Takemori MT (1982) Dynamic bulk and shear relaxation in glassy polymers. I. Experimental results and techniques on PMMA. J Appl Polym Sci 20:205–224. (physics edition)
4. Giovagoni M (1994) On the direct measurment of the dynamic Poisson's ratio. Mech Mater 17:33–46.
5. Delin M, Rychwalski R, Kubát J (1995) Volume changes during stress relaxation in polyethylene. Rheol Acta 34(2):182–195.
6. Tcharkhtchi A, Faivre S, Roy LE, Trotignon JP, Verdu J (1996) Mechanical properties of thermosets. Part I. Tensile properties of an anhydride cured epoxy. J Mater Sci 31:2687–2692.
7. Stokes VK, Nied HF (1988) Lateral strain effects during the large extension of thermoplastics. Polym Eng Sci 28(19):1209–1218.
8. Urayama K, Takigawa T, Masuda T (1993) Poisson's ratio of poly(vinyl alcohol) gels. Macromolecules 26:3092–3096.
9. Weber H, Wolf T, Dunger U (1997) Determination of relaxation moduli and Poisson's ratio in uniaxially loaded solid polyethylene foam specimens as part of full mechanical characterization. Mech Time-depend Mater 1:195–208.
10. Righetti R, Ophir J, Srinivasan S, Krouskop T (2004) The feasibility of using elastography for imaging the Poisson's ratio in porous media. Ultrasound Med Biol 30(2):215–228.
11. Krause I, Segreto AJ, Przirembel H, Mach RL (1966) Poisson's ratio of viscoelastic materials. Mater Sci Eng 1:239–250.
12. Tsou AH, Greener J, Smith GD (1995) Stress relaxation of polymer films in bending. Polymer 36(5):949–954.
13. Arzoumanidis GA, Liechti KM (2003) Linear viscoelastic property measurement and its significance for some nonlinear viscoelasticity models. Mech Time-depend Mater 7:209–250.
14. Ernst LJ, Zhang GQ, Jansen KMB, Bressers HJL (2003) Time- and temperature-dependent thermo-mechanical modeling of a packaging molding compound and its effect on packaging process stresses. J Electron Packag 125:539–548.
15. Lu H, Zhang X, Knauss WG (1997) Uniaxial, shear, and poisson relaxation and their conversion to bulk relaxation: studies on poly(methyl methacrylate). Polym Eng Sci 37(6):1053–1064.
16. Kugler HP, Stacer RG, Stemile C (1990) Direct measurement of Poisson's ratio in elastomers. Rubber Chem Technol 63(4):473–487.
17. Theocaris PS, Hadjijoseph Chr (1965) Transient lateral contraction ratio of polymers in creep and relaxation. Kolloid-Z Z Polym 202(2):133–139.
18. Theocaris PS (1979) Influence of plasticizer on Poisson's ratio of epoxy polymers. Polymer 20:1149–1152.
19. van der Varst PG Th, Kortsmit WG (1992) Notes on the lateral contraction of linear isotropic viscoelastic materials. Arch Appl Mech 62:338–346.
20. Hilton HH (2001) Implications and constraints of time-independent Poisson's ratios in linear isotropic and anisotropic viscoelasticity. J Elast 63:221–251.
21. Tschoegl NW (1989) The phenomenological theory of viscoelasticity. Springer, Berlin Heidelberg New York.
22. Shrotriya P, Sottos NR (2004) Local time-temperature dependent deformation of a Woven composite. Exp Mech 44:336–354.
23. O'Brien DJ, White SR (2003) Cure kinetics, glass transition, and gelation of EPON 862/W epoxy. Polym Eng Sci 43(4):863–874.
24. O'Brien DJ, Mather PT, White SR (2001) Viscoelastic properties of an epoxy resin during cure. J Compos Mater 35(10):883–904.
25. Post D, Han BF, Ifju P (1994) High sensitivity moiré. Springer, Berlin Heidelberg New York.
26. Trottle CR (1984) An encyclopedia of metallurgy and materials. MacDonald and Evans, Plymouth, UK.
27. Ferry JD (1980) Viscoelastic properties of polymers. Third edition. Wiley, New York.
28. Callister WD (1994) Materials science and engineering, an introduction. Wiley, New York.
29. Drozdov AD (2001) The nonlinear viscoelastic response of glassy polymers subjected to physical aging. Macromol Theory Simul 10(5):491–506.